Research Article | Vol. 10, No. 12 / 1 December 2019 / Biomedical Optics Express 6286

Biomedical Optics EXPRESS

75-degree non-mydriatic single-volume optical coherence tomographic angiography

XIANG WEI,[1,2] TRISTAN T. HORMEL,[1] YUKUN GUO,[1] AND YALI JIA[1,2,*]

[1]Casey Eye Institute, Oregon Health & Science University, Portland, OR 97239, USA
[2]Department of Biomedical Engineering, Oregon Health & Science University, Portland, OR 97239, USA
[*]jiaya@ohsu.edu

Abstract: Optical coherence tomography (OCT) and OCT angiography (OCTA) enable three-dimensional, high-resolution imaging of the eye. Yet, while they provide unprecedented structural and angiographic imaging detail, both have only limited fields of view in comparison to other imaging modalities like fundus photography. In this paper, we present a high-speed, high-sensitivity, swept source laser-based system that can acquire non-mydriatic 75-degree field of view OCT and OCTA images in a single complete scan without resorting to montaging techniques. The system uses an optimized scanning protocol and achieves capillary-level image quality. Such data may improve early detection of pathology and provide valuable information during disease monitoring.

1. Introduction

Optical coherence tomography (OCT) acquires three-dimensional, depth-resolved images of biological tissues [1]. OCT angiography (OCTA) has recently been developed to generate high-contrast, high-resolution angiograms by computing the OCT signal changes due to blood flow between temporally displaced B-scans [2–5]. As with OCT, it is three-dimensional and non-invasive [2–4,6] and has been successfully commercialized for imaging vascular abnormalities in ocular diseases [7].

Both OCT and OCTA are exceptionally powerful ophthalmic imaging techniques, but compared to many other imaging modalities (e.g., fluorescein angiography (FA) and fundus photography) they both suffer from a limited field of view. If the field of view of OCTA scan can be extended to the region accessed by FA and photograph, label-free OCTA will be extensively used for routinely screening and monitoring early diabetic retinopathy (DR) or inherited retinal diseases that frequently show the earliest site of dysfunction in the peripheral retina.

To capture a wide-field image, two constraints have to be considered. On one hand, OCT and OCTA image quality, particularly with respect to the strength of motion artifacts, is dependent on B-scan rate. This dependence is especially acute in OCTA, since any motion will also register as signal. A high B-scan rate is therefore required [8]. On the other hand, to maintain a high sampling density in a large field of view, many A-scans are required for each B-scan, consequently decreasing B-scan rate. A-scan rate, then, is of paramount importance for the design of wide-field OCTA imaging.

Current commercially available OCT systems can achieve 100-kHz A-scan rates. The fastest experimental systems use frequency tunable lasers [9] and can reach megahertz A-scan rates [10], with their speed limited by the repetition rate of the swept laser. The largest field of view achieved so far is 100 degrees [11]. The scanning method reported in the 100-degree field of view study is a bidirectional sinusoidal scanning pattern which introduced an uneven sampling density along the lateral direction. The study also didn't demonstrate a wide-field OCTA image.

Alternatively, wide-field OCTA images can be acquired by montage [12]. However, to use this technique, during the imaging session the patient has to rotate their eye according to the

#378073 https://doi.org/10.1364/BOE.10.006286
Journal © 2019 Received 17 Sep 2019; revised 11 Nov 2019; accepted 11 Nov 2019; published 15 Nov 2019

Biomedical Optics EXPRESS

position of a fixation target. For anything larger than a 60-degree field of view, many images are typically required for montage. This will increase the imaging time and decrease the comfort of the patient, as well as producing more artifact-rich images. Montaging itself also provides a new means for introducing artifacts, since image stitching may not always be perfectly executed. Ultimately all of these issues may lead to fewer successful image acquisitions, undercutting the utility of the approach.

Currently, wide-field images are usually taken after dilation. As a routine ophthalmic procedure, dilation can introduce some side effects and discomfort. A non-mydriatic single-volume wide-field OCTA imaging method obviates many of these concerns. Since montage is not required, no scans will be ruined by incorrect image stitching. And acquisition is not as arduous for patients. However, single-volume imaging introduces its own challenges: high A-scan rates have an additional premium since a large number of A-scans must be captured during a single volumetric scan. Furthermore, larger fields of view can introduce severe vignetting artifacts. In this work, we address these issues through the use of an improved optical design and an innovative scan pattern to obtain single-volume wide-field high resolution OCT and OCTA scans.

2. Methods

2.1. 400-kHz swept-source laser

A 400-kHz swept-source laser (AXSUN Technologies, USA) was used in this study. It has a center wavelength of 1060 nm with a 100 nm swept range. The theoretical maximum axial resolution is 5 μm in the air. It contains two 200-kHz micro-electro-mechanical system (MEMS) based tunable short cavity swept-source lasers operating at a 50% duty cycle. By triggering these two lasers at different times, they can be combined to achieve a 400-kHz swept speed at 100% duty cycle. Due to the birefringence introduced by the optical fiber inside the laser engine, the output laser has two different polarization states corresponding to the two different lasers. Two three paddle manual polarization controllers (Thorlabs, Inc., USA) were applied separately in both the sample and reference arms to eliminate polarization differences. The laser does not have a built-in sampling clock. Therefore, a Mach-Zehnder interferometer-based sampling clock generator was built to provide a high-speed k-space clock. We achieved 1536 sampling points per sweep for each A-scan. The maximum image depth is 4.2 mm in the air and 3 mm in tissue. The reference arm was built using a custom motorized optical delay line with tunable range of 100 mm.

2.2. Reduction of vignetting artifacts

Vignetting artifacts are very common during OCT imaging [13]. The common cause, particularly in absence mydriasis, is the iris blocking the probe laser during part of the scan. Vignetting artifacts can also be generated by misalignment between the OCT system and patient's pupil. The misalignment will cause partial defocusing of the scanning area, which causes vignetting. Wide-field imaging is especially sensitive to vignetting from both of these causes, so extra care needs to be taken to ensure that the scanning focal point of the OCT system is accurately positioned in the center of pupil. However, the fast mirror and slow mirror of a conventional galvo scanner are separate components (Fig. 1(A)). This will cause the scanning focal points of these two mirrors to be located at different axial positions on the pupil. For example, if we precisely position the scanning focal point of the fast mirror on the pupil, the scanning focal point from the slow mirror may not always be on the pupil, and so part of the light in the slow axis direction will be blocked (Fig. 1(B)). Since the blocked region will have no back scattered signal, it will appear as a black region in the cross sectional and *en face* OCT images (Fig. 1(C)). If the system is built using commercially available lenses the vignetting artifact will first appear in the near center part of the image because the focal points depend on the scanning angle. The focal

Biomedical Optics EXPRESS

length is shorter on a large scanning angle than on a small scanning angle. This allows the laser beam from both large and small angles to pass through the pupil, but the beam from intermediate angles is blocked. Simulations performed in OpticStudio (Zemax, LLC., USA) show vignetting artifacts on two commercially available lenses (Fig. 1(D), (E)). The vignetting artifact and its axis dependency can also be observed by imaging a 3D printed model eye with a 3 mm pupil size (Fig. 1(F)). Our model eye contains a spherical inner surface and a half inch 19 mm achromatic doublet lens. We acquired an *en face* projection image (Fig. 1(G)) from a 75-degree field of view OCT image of the model eye. The slow axis cross sectional image has no vignetting artifacts (Fig. 1(H)), but the fast axis cross sectional image has a symmetric vignetting artifact due to the misalignment (Fig. 1I).

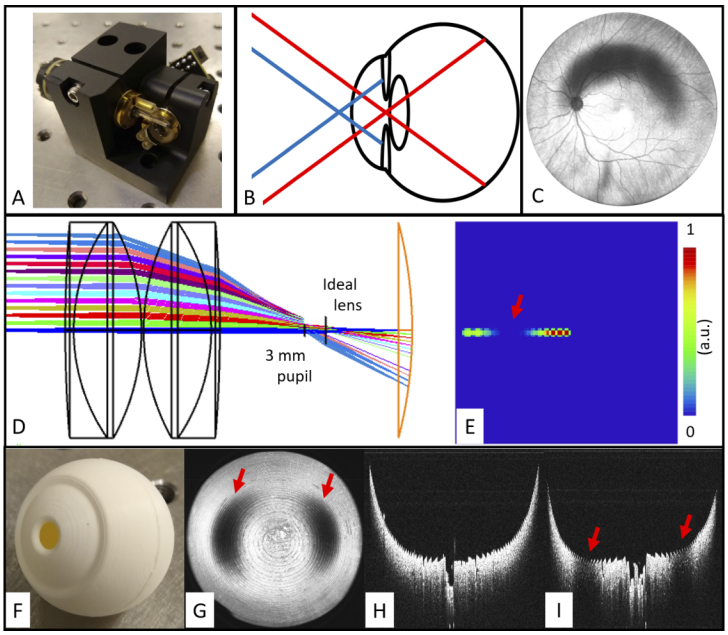

Fig. 1. (A) 3D model of conventional galvo scanner setup. (B) Diagram of different scanning focal lengths on different axes; red light indicates the fast axis and blue light indicates the slow axis. (C) Health human OCT *en face* image with vignetting artifacts. (D) OpticStudio (Zemax, LLC) simulated ray tracing results with two 80 mm achromatic doublets (Thorlabs Inc.). (E) Energy map of the imaging plane. The red arrows indicate rays affected by vignetting artifacts. (F) 3D printed eye model with 3 mm pupil size. (G) wide-field *en face* image of the model eye. (H) vertical axis cross sectional image. (I) horizontal axis cross sectional image.

To compensate for the difference between the fast and slow scanning focal lengths, we applied an additional 4f-system to project the X scanner on to the Y scanner (Fig. 2(A)). A 4f-system is an optical setup that contains two sets of lenses with the output focal plane of the first lens overlaid with input focal plane of the second lens. The magnification of the system is defined by the focal length ratio of these two lenses. The additional 4f-system was built using two sets of combined achromatic doublet lenses with a 33 mm effective focal length; the magnification of this setup is unity. By using this system, we can ensure that there will be no scanning focal point difference on the pupil and the axis-dependent vignetting artifact will be eliminated. This also decreases the difficulty of alignment for OCT operator.

Biomedical Optics EXPRESS

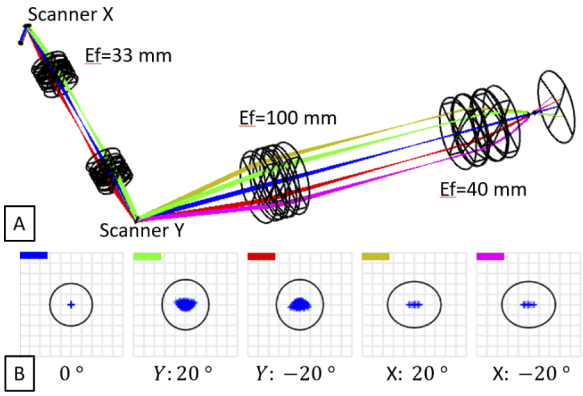

Fig. 2. (A) Schematic of the OCT sample arm with optical relay, with effective focal length Ef. Different color rays denote different scanning angles. (B) Spot diagrams of five different scanning angles, simulated in OpticStudio (Zemax, LLC). The color bar on the left corresponds to the ray colors in (A).

2.3. Simulation

The performance of the optical system was simulated and evaluated using OpticStudio (Zemax, LLC., USA). The simulated system contains a telescope system and a 4f optical relay. The telescope system has two sets of two-inch 200 mm achromatic doublet lenses with 100 mm effective focal length, and two sets of two-inch 80 mm achromatic doublet lenses with 40 mm effective focal length. By using the telescope system, the scanning angle is amplified 2.5 times, from the original 30 degrees out of the galvo scanner to a maximum scanning angle of 75 degrees. The 4f optical relay is simulated according to the setup described previously. The ray tracing spot diagram was studied according to different scanning angles in the X and Y direction. Spot diagrams at five different positions (0°, ±20°X, ±20°Y) were simulated. The spot diagrams show the distribution of ray tracing spots are all within the optical system's diffraction limit even with large scanning angles (Fig. 2(B)).

2.4. Mechanical design of the wide-field sample arm

A 400-kHz wide-field OCT system was modified from a previously reported system [14]. First, 10% of the light from the laser is split to the sampling clock interferometer using a fiber optic coupler. The sampling clock interferometer includes two optical delay lines and a 1 GHz balanced photodetector. The remaining 90% of the light is split at a 40/60 ratio to the sample and reference arm. The reference arm contains a polarization controller and a motorized delay line controlled by a microcontroller. The same microcontroller is also used to control the fixation target screen in the sample arm. A dichroic mirror (Chroma, USA) is used to couple the fixation target and the camera to the optical axis (Fig. 3).

The wide-field sample arm was designed using computer aided design (CAD) software (SolidWorks, Dassault Systèmes, France) with 3D printed optical mounts. The position and height of each optical mount was precalculated. The accuracy of the 3D printer is greater than 100 µm. This allows us to assemble the sample arm with minimal alignment work. The dispersion is compensated using both digital and physical methods. The sample arm power is limited to 2 mW on the pupil. The sensitivity of the system was measured using a set of neutral density filters and a silver mirror. By precisely controlling the length of the reference arm delay line, the sensitivity at different depths can be measured (Fig. 4(B)). The maximum sensitivity was measured to be 102.4 dB at 0.2 mm depth, the minimum sensitivity is 101.2 dB at imaging depth

Biomedical Optics EXPRESS

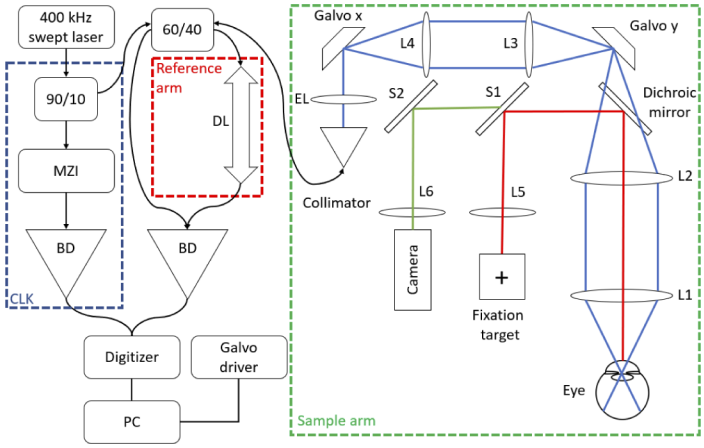

Fig. 3. Diagram of the wide-field OCT system used in this study. A 400-kHz swept-source laser is the light source. A Mach-Zehnder interferometer provides the sampling clock (CLK). A delay line (DL) is used to adjust the reference arm length. A 40 mm effective focal length lens (L1) provides the 75-degree scanning angle inside the pupil. Other optical elements used in the system are: L2: 100 mm effective focal length lens, L3, L4: 33 mm effective focal length lenses, L5 and L6 zoomable lenses, S1: 50:50 beam splitter, S2: silver mirror, EL: electric lens. System output is produced by a balanced photodetector (BD) which converts the optical signal to an electrical signal. The signal is digitized using a digitizer and collected by a computer (PC).

of 4.2 mm, giving a signal roll-off of 1.2 dB across a 4 mm imaging depth. The high sensitivity of this system ensures image quality during wide-field imaging.

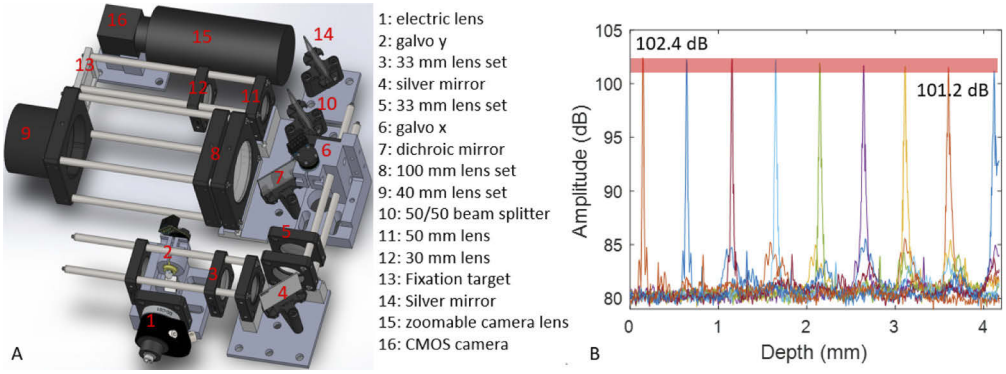

Fig. 4. (A) 3D rendered model (Solidworks, Dassault Systèmes) of the sample arm according to the design schematic in Fig. 3. Due to the size limitations, the optical relay is folded using a silver mirror. Grey colored parts are customized optical mounts which need to be 3D printed; other parts are either provided by the manufacture or designed according to hardware requirements. (B) Sensitivity roll-off across the whole imaging depth. Different colors indicate different depths. The red shaded are at the top indicates the signal roll off across the 4 mm imaging depth.

2.5. *Bidirectional scanning pattern*

Wide-field OCT imaging requires both high-density scans and a large field of view. These requirements will increase the total scanning time during data acquisition. Compared to a narrow-field image, the scanning efficiency is more important in a wide-field scan since mechanical adjustments are larger and, if resolution is to be maintained, a larger number of A-scans are

Biomedical Optics EXPRESS

required. A raster scanning pattern is the conventional scanning pattern used in many instruments. It contains a forward scan and a backward scan. The forward scan is used to acquire the image data, but the backward scan points, commonly referred to as fly back points, cannot be used to acquire effective imaging data. Wide-field OCT systems require longer fly-back due to the large scan region, which makes raster scan patterns more inefficient. In our system a highly efficient bidirectional scanning pattern was used to maximize the effective data acquisition time [15]. This scanning pattern does not need fly-backs to reset the scanner, which saves more than 25% of the total scanning time. Another benefit of this scanning pattern is the tunable scanning interval, which can be modified to maximize the sensitivity to flow dynamic range. Compared to a traditional raster scanning pattern, this bidirectional scanning pattern requires a faster and more accurate response driver. A set of high speed galvo scanners (ScannerMax, Pangolin Laser Systems Inc., USA) were used. The scanners are controlled by a digital driver with a pseudo derivative feedback (PDF) controller integrated. Compared to conventional proportional-integral-derivative (PID) controllers, PDF controllers can ensure both a fast response and highly accurate scanning [16].

3. Results

3.1. 75-degree retinal image

Application of a fast 400-kHz swept-source laser enabled wide-field high-density scanning. In this study, a 28-year-old male healthy human retinal image was acquired in a dark room (Fig. 5(A)), the pupil diameter was measured to be 5 mm. The scanning field of view is 75 degrees, which is equivalent to 23 × 23-mm. 1536 A-scans were acquired for each B-scan. A total of 1536 B-scans were acquired across 768 cross sectional positions. At each location, two repeats were acquired, which enabled the generation of high-resolution OCTA images. The total scanning time was 5.9 seconds.

Benefitting from the short scanning time and the precise alignment, no obvious vignetting artifacts can be observed on OCT *en face* images (Fig. 5(A)). The retinal layer structure is

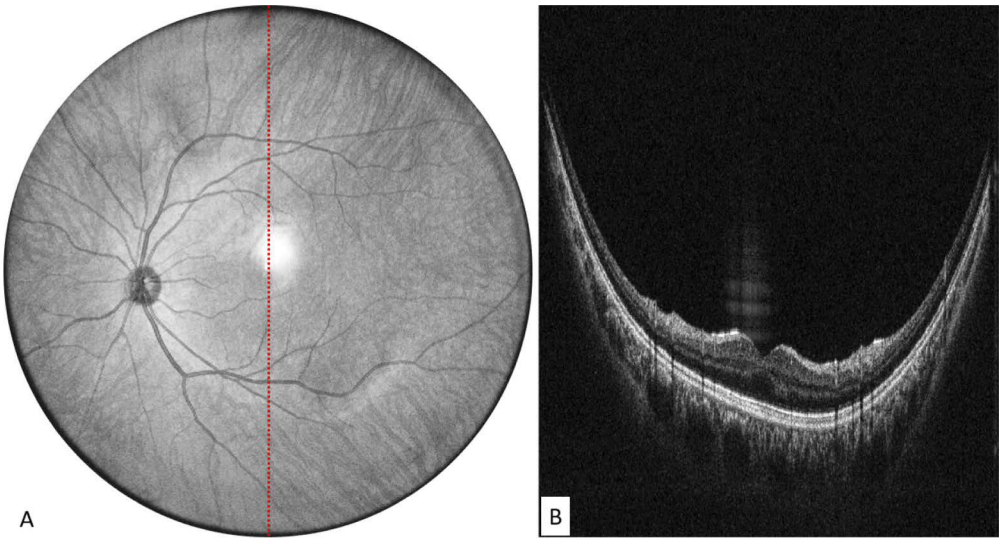

Fig. 5. (A) 75-degree OCT retinal structure image generated using full intensity projection. The dashed red line indicates the location of the cross-sectional image location. (B) Cross sectional retinal image.

Biomedical Optics EXPRESS

distinguishable in both macular region and peripheral region (Fig. 5(B)). Due to the curvature of the retina and the relatively large aberrations at the edge of the lens, very thin black borders can be visible on the boundary of images.

In both wide-field OCT/OCTA, segmentation is the must-have step, but is very challenging. In our study, an automatic segmentation algorithm was applied [17] and assisted by minor manual correction. An image of the choroid was generated by minimum projection of the OCT structural image through Sattler's layer and Haller's layer (Fig. 6(A)). The image shows high contrast between the vessels and the background. Medium and large vessels are visible in this image. OCTA images can also be generated from the same data set by calculating the decorrelation between two repeated scans (Fig. 6(B)). The split spectrum amplitude decorrelation algorithm [4] was applied to the raw spectrum. By applying the results of the automatic segmentation, an inner retinal OCTA image was generated using maximum value projection without additional image

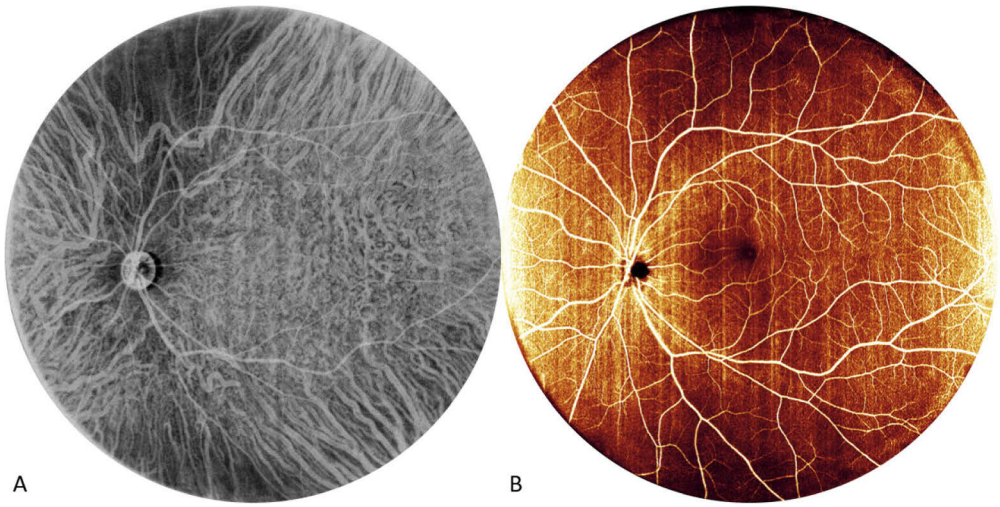

Fig. 6. (A) Structural OCT of the choroid, showing dense vasculature, (B) OCTA of the inner retina.

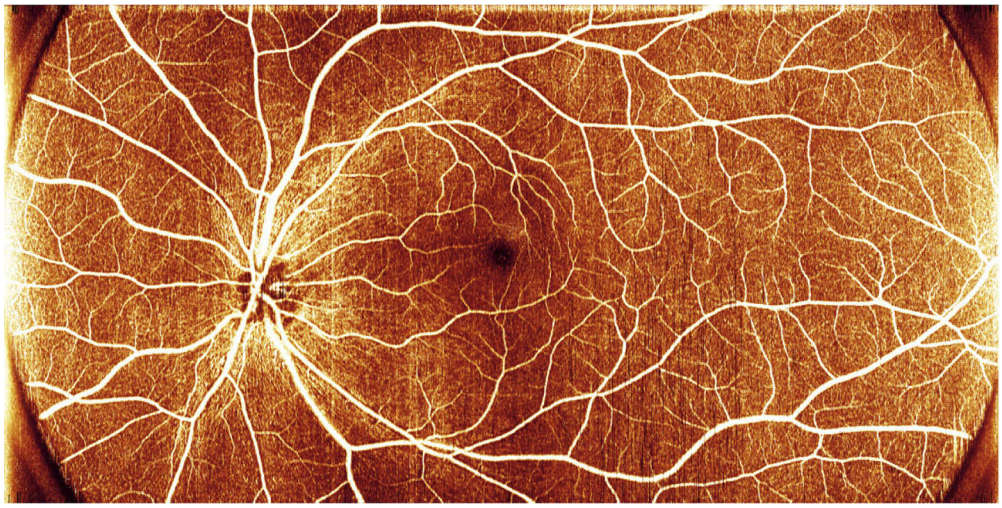

Fig. 7. High-resolution OCTA (12 × 23-mm).

Biomedical Optics EXPRESS

processing method [18], the brightness and contrast have been adjusted for better visualization. The full view of microcirculation at back of the eye can be observed - high blood supply at the peripapillary region and small avascular region at fovea. Although the distribution of the large and medium vessels can be clearly visualized (Fig. 6(B)), the capillary vasculature is not directly discernible due to under sampling in the scanning area.

Resolution can be increased to view capillary details by either increasing the sampling density or reducing the field of view. A higher sampling density would require a faster laser or longer scanning time. Instead, we reduced the vertical field of view while keeping the horizontal intact, focusing on the posterior pole region (Fig. 7). Using the same number of A-scans on each B-scan as previous image (Fig. 6(B)), we can generate a sampling step of 15 μm in both the fast and slow axis. Our experiment (Fig. 7) indicates capillary resolution was achieved.

4. Discussion

We achieved wide-field, non-mydriatic high-resolution structural OCT and OCTA imaging with high-speed data acquisition using a novel bidirectional scan pattern and a high-speed 400-kHz swept-source laser. In this study, the high-resolution OCTA image was acquired within 6 seconds with a highly efficient bidirectional scanning pattern. The optimized optical system design with separated XY scanners minimized the alignment difficulty and eliminated vignetting artifacts. Over 100 dB sensitivity was achieved, which provides the possibility of high-quality imaging. The system achieved capillary scale resolution in a 12×23-mm OCTA image.

Due to the limitation of under-sampled scanning, capillary fine details could not be clearly appreciated on the full 75-degree field of view, and the image resolution was lower than in 3×3-mm OCTA scans provided by most commercial systems; nonetheless we anticipate that it would allow us detect common vascular pathologies (e.g., non-perfusion area or neovascularization). Still, for many applications capillary detail is desirable, if not essential. One solution is to use the near capillary resolution wide-field OCTA image as a guiding image (Fig. 8(A)), and once a potentially abnormal area is noticed, a high-resolution, narrow-field OCTA image of the pathological region could be acquired (Fig. 8(B)).

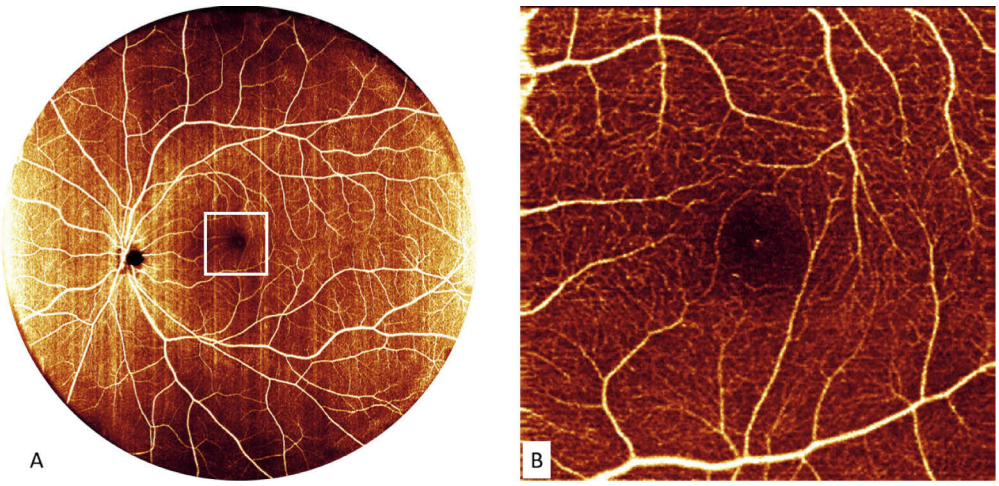

Fig. 8. (A) 75-degree wide-field OCTA image, with white box indicating the area of interest. (B) High resolution 10-degree (3 × 3 mm) field of view OCTA image acquired within the white box in (A). The image in (B) contains 304 A-scan per B-scan, and 912 B-scans with 2 repeats, captured with a total acquisition time is 1.4 s.

Biomedical Optics EXPRESS

Another way to acquire capillary level resolution is to increase the sampling density; in our instrument, this would require doubling the sampling density in either the fast or slow direction. The consequence is an increase in the total scanning time. Since there is no tracking system provided in this prototype, further extension of acquisition time is not a viable solution.

It therefore seems further increasing the speed of the laser is a more appropriate way to proceed. Since OCTA imaging requires a minimum of two complete scans in order to obtain flow contrast, this means doubled OCTA sampling density requires quadrupling the system speed in order to retain the same scanning time. Ultrahigh-speed systems introduce their own challenges. With scanning rates getting faster, the number of photons received by the detector per unit time is smaller, and the sensitivity of the system needs to be boosted to compensate for the photon loss.

Aberrations are another problem for wide-field OCTA imaging. In our system, due to the optical relay and the short focusing on a large scanning angle, there are relatively large aberrations at the upper and lower edge of the OCTA image. This artifact is hard to observe on a structural image due to lower sensitivity to vignetting artifacts. This type of artifact can be compensated for by either applying a custom designed lens or applying a long focal length and large diameter lens in the optical relay system.

Finally, high-speed systems will also introduce challenges for the scanning system itself. The scanner needs to have a high response frequency throughout a large scanning angle. Resonate galvo scanners and MEMS scanner are available for this purpose. However, both resonate galvo scanners and MEMS scanners have nonlinear responses, which will lead to more image distortion compared to conventional galvo scanners. Correcting for distortion will sacrifice some resolution. A precise linear scanning control system will be needed for future high-speed applications to adapt to high-speed scanning.

5. Conclusion

Field of view is one of the key limitations in OCT systems. In order to overcome this limitation, we included several design improvements into a custom 400 kHz swept source laser instrument. Among these improvements are (1) we designed an OCT sample arm optimized for wide-field applications; (2) to avoid vignetting, and decrease the difficulty of aligning the system, we used a novel optical relay; and (3) to maximize scanning efficiency we applied a bidirectional scanning pattern. Using this system, we successfully obtained 75-degree field of view and, with a slightly restricted field of view, capillary scale detail in OCTA images from a healthy human subject.

Funding

National Institutes of Health (P30 EY010572, R01 EY024544, R01 EY027833); Research to Prevent Blindness (unrestricted departmental funding grant, William & Mary Greve Special Scholar Award).

Disclosures

Oregon Health & Science University (OHSU) and Yali Jia have a significant financial interest in Optovue, Inc. These potential conflicts of interest have been reviewed and managed by OHSU.

References

1. D. Huang, E. A. Swanson, C. P. Lin, J. S. Schuman, W. G. Stinson, W. Chang, M. R. Hee, T. Flotte, K. Gregory, and C. A. Puliafito, "Optical coherence tomography," Science **254**(5035), 1178–1181 (1991).
2. S. Makita, Y. Hong, M. Yamanari, T. Yatagai, and Y. Yasuno, "Optical coherence angiography," Opt. Express **14**(17), 7821–7840 (2006).
3. L. An and R. K. Wang, "In vivo volumetric imaging of vascular perfusion within human retina and choroids with optical micro-angiography," Opt. Express **16**(15), 11438–11452 (2008).

Biomedical Optics EXPRESS

4. Y. Jia, O. Tan, J. Tokayer, B. Potsaid, Y. Wang, J. J. Liu, M. F. Kraus, H. Subhash, J. G. Fujimoto, and J. Hornegger, "Split-spectrum amplitude-decorrelation angiography with optical coherence tomography," Opt. Express **20**(4), 4710–4725 (2012).
5. A. Mariampillai, B. A. Standish, E. H. Moriyama, M. Khurana, N. R. Munce, M. K. Leung, J. Jiang, A. Cable, B. C. Wilson, and I. A. Vitkin, "Speckle variance detection of microvasculature using swept-source optical coherence tomography," Opt. Lett. **33**(13), 1530–1532 (2008).
6. T. E. De Carlo, A. Romano, N. K. Waheed, and J. S. Duker, "A review of optical coherence tomography angiography (OCTA)," Int. J. Retin. Vitr. **1**(1), 5 (2015).
7. I. Gorczynska, J. V. Migacz, R. J. Zawadzki, A. G. Capps, and J. S. Werner, "Comparison of amplitude-decorrelation, speckle-variance and phase-variance OCT angiography methods for imaging the human retina and choroid," Biomed. Opt. Express **7**(3), 911–942 (2016).
8. R. F. Spaide, J. G. Fujimoto, and N. K. Waheed, "Image artifacts in optical coherence angiography," Retina **35**(11), 2163–2180 (2015).
9. S. Chinn, E. Swanson, and J. Fujimoto, "Optical coherence tomography using a frequency-tunable optical source," Opt. Lett. **22**(5), 340–342 (1997).
10. T. Klein, W. Wieser, C. M. Eigenwillig, B. R. Biedermann, and R. Huber, "Megahertz OCT for ultrawide-field retinal imaging with a 1050 nm Fourier domain mode-locked laser," Opt. Express **19**(4), 3044–3062 (2011).
11. J. P. Kolb, T. Klein, C. L. Kufner, W. Wieser, A. S. Neubauer, and R. Huber, "Ultra-widefield retinal MHz-OCT imaging with up to 100 degrees viewing angle," Biomed. Opt. Express **6**(5), 1534–1552 (2015).
12. Q. Zhang, C. S. Lee, J. Chao, C.-L. Chen, T. Zhang, U. Sharma, A. Zhang, J. Liu, K. Rezaei, and K. L. Pepple, "Wide-field optical coherence tomography based microangiography for retinal imaging," Sci. Rep. **6**(1), 22017 (2016).
13. X. Wei, A. Camino, S. Pi, T. T. Hormel, W. Cepurna, D. Huang, J. C. Morrison, and Y. Jia, "Real-time cross-sectional and en face OCT angiography guiding high-quality scan acquisition," Opt. Lett. **44**(6), 1431–1434 (2019).
14. X. Wei, T. T. Hormel, S. Pi, Y. Guo, Y. Jian, and Y. Jia, "High dynamic range optical coherence tomography angiography (HDR-OCTA)," Biomed. Opt. Express **10**(7), 3560–3571 (2019).
15. M. J. Ju, M. Heisler, A. Athwal, M. V. Sarunic, and Y. Jian, "Effective bidirectional scanning pattern for optical coherence tomography angiography," Biomed. Opt. Express **9**(5), 2336–2350 (2018).
16. W. R. Benner, *Laser Scanners: Technologies and Applications; how They Work, and how They Can Work for Your Product* (Pangolin, 2016).
17. Y. Guo, A. Camino, M. Zhang, J. Wang, D. Huang, T. Hwang, and Y. Jia, "Automated segmentation of retinal layer boundaries and capillary plexuses in wide-field optical coherence tomographic angiography," Biomed. Opt. Express **9**(9), 4429–4442 (2018).
18. T. T. Hormel, J. Wang, S. T. Bailey, T. S. Hwang, D. Huang, and Y. Jia, "Maximum value projection produces better en face OCT angiograms than mean value projection," Biomed. Opt. Express **9**(12), 6412–6424 (2018).